ADVANCED MATERIALS

DOI: 10.1002/adma.200702930

Universal Block Copolymer Lithography for Metals, Semiconductors, Ceramics, and Polymers**

By *Seong-Jun Jeong, Guodong Xia, Bong Hoon Kim, Dong Ok Shin, Se-Hun Kwon, Sang-Won Kang,* and *Sang Ouk Kim**

Nanostructured thin films of metals, semiconductors, ceramics, and polymers have demonstrated a variety of attractive properties owing to the dramatic increase of the surface area and quantum confinement in the nanoscale geometry.[1,2] Because of their novel properties, the nanostructured films are anticipated to be useful for numerous next-generation devices such as sensors,[3] electronic or photonic devices,[4,5] catalysts,[6] etc. To date, various film deposition methods such as sol-gel spin-casting,[7] sputtering, chemical vapor deposition (CVD),[8] or atomic layer deposition (ALD)[9,10] have been developed, providing a fine tunability over the film thickness, even on the sub-nanometer scale.[1,2,11] However, in order to generate the nanoscale structure in the lateral dimension, a nanolithographic process must be applied.

Electron beam lithography and nanoimprinting are widely utilized nanolithographic processes that may overcome the resolution limit of conventional photolithography. However, their serial writing process or direct mechanical contact with a target material frequently limits large-scale production of densely packed nanostructures.[12,13] Alternatively, nanoporous templates, such as track-etched membrane or anodic aluminum oxide (AAO), have been used in conjunction with a deposition or etching process to produce various nanostructured materials.[14] Although track-etched membranes and AAO are commercially available, they only provide porous template morphology. In addition, their adhesion with a substrate is generally poor, and severe chemical processes are required to remove them after the fabrication process.[15]

[*] Prof. S. O. Kim, S.-J. Jeong, Dr. G. Xia, B. H. Kim, D. O. Shin, Dr. S.-H. Kwon, Prof. S.-W. Kang
Department of Materials Science and Engineering
KAIST Institute for the Nanocentury, KAIST
Daejeon 305-701 (Korea)
E-mail: sangouk.kim@kaist.ac.kr

[**] We thank G. S. Kim and J.-H. Ahn for assistance with thin film depositions, and S. S. Bae for assistance with SEM analysis. This work was supported by the second stage of the Brain Korea 21 Project, the Korea Research Foundation (KRF-2005-003-D00085), the Basic Research Program of the Korea Science & Engineering Foundation (R01-2005- 000-10456-0), the Korean Ministry of Science and Technology, and the Korean Ministry of Science and Technology and Fundamental R&D Program for Core Technology of Materials funded by the Korean Ministry of Commerce, Industry and Energy. Also, this work was partially supported by grants-in-aid for the National Core Research Center Program from MOST/KOSEF (No. R15-2006-022-01001-0).

Block copolymer lithography is an emerging nanolithographic process utilizing self-assembled nanoscale morphologies of block copolymers. Unlike commercially available nanoporous templates, block copolymers may provide diverse shapes of nanostructures, including spheres, cylinders, lamellae, or interconnected networks with fine tunability over their sizes.[16,17] The self-assembled block copolymer nanotemplates generally have a good adhesion with a substrate surface and can be easily removed by a mild chemical or radiative treatment after a fabrication process. Furthermore, directed assembly techniques such as epitaxial self-assembly[18–20] or graphoepitaxy[21,22] have been developed to provide well-ordered device-oriented nanostructures. Despite the numerous advantages, however, block copolymer lithography has been mostly applied to silicon based substrates so far, which is largely due to the difficulty in controlling the orientation and lateral ordering of self-assembled nanoscale morphologies upon an arbitrary substrate.[23] To prepare the well-ordered high-aspect-ratio block copolymer nanotemplates consisting of surface perpendicular lamellae or cylinders, the surface tension of the underlying functional material has to be adjusted by a surface treatment. For the development of various nanoscale devices, a general approach widely applicable to a spectrum of functional materials is required.[24–27]

We introduce a universal block copolymer lithography process for arbitrary functional materials. A hybrid approach combining advanced film deposition processes, such as sputtering, CVD, sol-gel spin-casting, or ALD, with block copolymer lithography enabled a nanolithographic process applicable to most part of functional materials. Table 1 summarizes the wide range of functional materials applied in our work, which includes metals, semiconductors, ceramics, and even polymers. Metals are generally electrically conductive, but their native oxides at the surfaces can be dielectric, semiconductive, or conductive. The ceramic materials such as nitrides or oxides cover as a broad spectrum of electric conductivity and functionality, including photocatalytic[28] and electro-light-emitting[29] properties. In order to prepare a well-ordered block copolymer nanotemplate in an equilibriated morphology, the substrate material must have reactive functional groups for surface modification as well as extremely low surface roughness. Film deposition techniques such as sputtering, ALD, PEALD, CVD, and sol-gel casting ensured nanometer scale film roughness. The surface functionality is given by the reactive hydroxyl group at the oxide surfaces. For

 WILEY InterScience DISCOVER SOMETHING GREAT © 2008 WILEY-VCH Verlag GmbH & Co. KGaA, Weinheim

Table 1. The functionalities, deposition process, and thickness of the various materials applied in this work.

	Substrate (Oxide)	Function	Deposition Process	Thickness [a] / RMS [b] [nm]	Native Oxide Thickness [c] [Å]
Metal	Cu (CuO)	Conductive Wire (P-type semiconductor)	Sputtering	100/0.691	23.39
	Ru (RuO_2)	Conductive Wire (Conductive Wire)	PEALD	60/1.153	17.35
	Ir (IrO_2)	Conductive Wire (Conductive Wire)	PEALD	60/1.199	3.26
	Pt (PtO_2)	Conductive Wire Electrocatalystic (Conductive Wire)	Sputtering	100/0.862	11.04
	$Co_{40}Fe_{60}$ (Co–Fe–O)	Ferromagnetic (Ferromagnetic)	Sputtering	30/0.926	12.09
Ceramic	Si_3N_4 (Si_2N_2O/SiO_2)	Dielectric (Refractory/Dielectric)	PECVD	40/0.203	1.71
	TiO_2	Photocatalyst Semiconductor	ALD	50/4.451	
	ZnO	Transparent & Light Emitting Semiconductor	Sol-Gel	60/0.869	
	HfO_2	High-*k* Dielectric	PEALD	35/0.427	
	In–Sn–O	Transparent Conductive Film	Sputtering	200/0.251	
Polymer	Polyimide	Flexible Dielectric	Solvent Casting	25 μm/1.136	

[a] Thicknesses of the thin films were measured by scanning electron microscopy (SEM) and spectroscopic ellipsometry. [b] RMS values were measured by atomic force microscopy (AFM). [c] Thicknesses of native oxide were measured by spectroscopic ellipsometry and reflectometry.

non-oxide materials, such as metals, semiconductors, or nitrides, thin native oxide layers were spontaneously formed on their surfaces in an atmospheric condition. Because the native oxide layer is spontaneously formed on most inorganic non-oxide materials, our strategy is universally applicable to most functional inorganic materials except for a few inert materials, such as gold.[30]

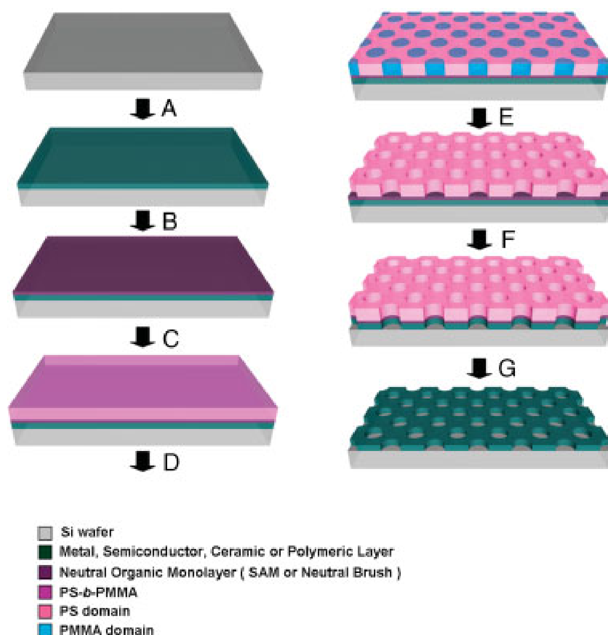

Figure 1. Schematic representation of the universal block copolymer lithography process. A) A target material film having a uniform thickness is deposited onto a silicon substrate and pretreated to induce a high density of chemical functionality at its surface. B) A SAM or PS-*r*-PMMA is deposited onto the substrate. C,D) A PS-*b*-PMMA copolymer is spin-coated onto a neutrally modified surface and thermally annealed to produce a self-assembled nanotemplate with surface perpendicular cylinders or lamellae. E) The PMMA component in the nanotemplate is selectively removed by a wet-etching process. F) The resultant nanostructured polystyrene template is applied as an etching mask for reactive ion etching (RIE) or ion milling. G) After removing the remaining block copolymer template, nanostructured films of various functional materials are produced.

The overall nanolithography process is schematically described in Figure 1. Firstly, a functional substrate with uniform thickness was deposited on a silicon substrate by sputtering, CVD, sol-gel spin-casting, or ALD. The deposited film was acid/base treated or ultraviolet oxygen (UVO) radiated to increase the reactive hydroxyl functional groups as well as to remove any organic contaminant at its oxide surface. The pretreated surface was covalently modified by a phenethyltrichlorosilane (PETS) self-assembled monolayer (SAM) or PS-*r*-PMMA random copolymer. After the organic modification, a PS-*b*-PMMA copolymer thin film was spin-coated and annealed at a high temperature. Since the organically modified surfaces had an identical interfacial tension to polystyrene (PS) and poly(methyl methacylate) (PMMA), the block copolymer thin film spontaneously assembled into a surface perpendicular morphology of lamellae or cylinders, providing a nanotemplate with a high aspect ratio and sharp pattern edge in an equilibrated morphology.[31,32] After self-assembly, the PMMA component was selectively wet-etched or degraded by UV radiation to reduce the resistivity to a subsequent etching process. Finally, a reactive ion etching (RIE) or ion-milling process was applied to transfer the nanoscale morphology of the block copolymer template into the underlying substrate material. After removing any remaining block copolymer nanotemplate, nanostructured films of various functional materials were produced.

As described above, acid/base or UVO pretreatment was applied to remove contaminants and to enhance surface functionality. Figure 2 shows X-ray photoelectron spectroscopy (XPS) spectra of iridium (Ir) and silicon nitride (Si_3N_4) films before and after the pretreatment process. As shown in Figure 2A, the O1s peak of the Ir film consisted of the IrO_2 peak (530.7 eV) and the $Ir(OH)_4$ peak (531.9 eV) of the native oxide layer.[33] The relative intensity of the $Ir(OH)_4$ peak

 © 2008 WILEY-VCH Verlag GmbH & Co. KGaA, Weinheim

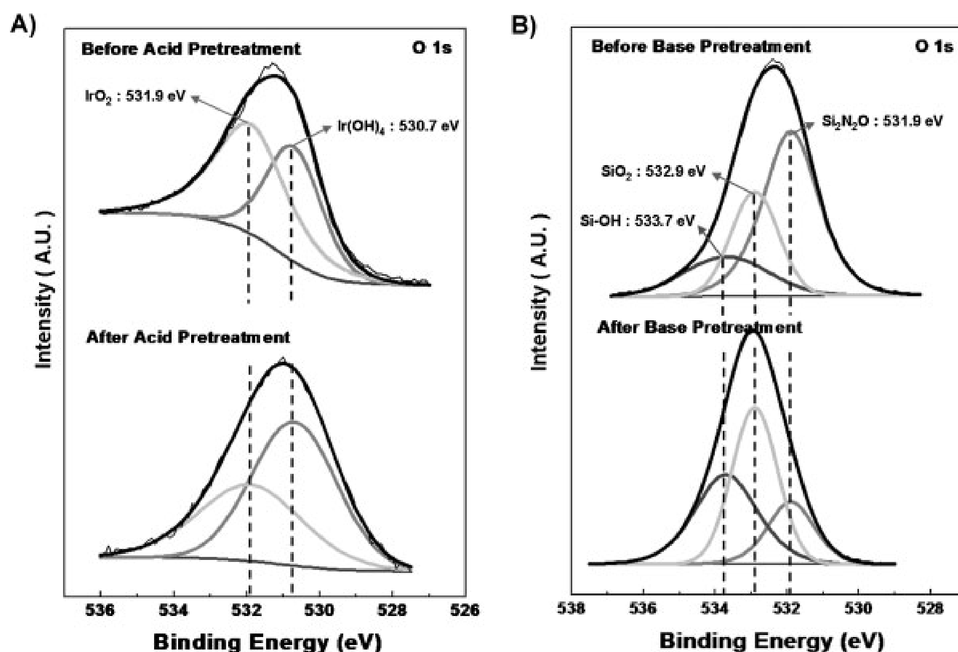

Figure 2. The X-ray photoelectron spectroscopy (XPS) O1s peaks of Ir and Si_3N_4 films before and after A) acid and B) base pretreatment processes.

increased remarkably after the acid pretreatment, confirming the enhancement of surface functionality. In Figure 2B, the O1s peaks of Si_3N_4 film consisted of the Si_2N_2O peak (531.9 eV), SiO_2 peak (532.9 eV), and Si–OH peak (533.7 eV) of the native oxide layer.[34] The growth of the Si–OH peak confirmed the increase of hydroxyl functional groups after base pretreatment. The influence of the pretreatment process upon the surface functionality could also be manifested by contact angle measurement, as summarized in Table 2. The water contact angle upon an as-deposited film surface ranged from 40° to 80°. This angle dramatically decreased to only a few degrees after pretreatment process owing to the increase of polar hydroxyl groups at the surface. Note that the polyimide, an inert organic material could be successfully surface-functionalized by UVO radiation without any significant damage to the material itself. All functional films exhibited a water contact angle of $80^\circ \pm 2^\circ$ after covalent modification with PETS SAM or PS-*r*-PMMA, demonstrating a neutrality to PS and PMMA components.[32]

Table 2. The variation of advancing water contact angles upon diverse functional materials at each stage of surface treatment process.

	Substrate (Oxide)	As-prepared Surface	Pretreatment UVO/Base[a]/Acid[b]			Neutral Organic Monolayer PS-*r*-PMMA/PETS	
Metal	Cu (CuO)	73° ± 3°	19°	–	–	81° ± 1°	–
	Ru (RuO_2)	64° ± 2°	1°	10°	1°	78° ± 1°	82° ± 2°
	Ir (IrO_2)	48° ± 3°	2°	2°	4°	82° ± 1°	–
	Pt (PtO_2)	59° ± 1°	4°	9°	–	81° ± 1°	79° ± 2°
	$Co_{40}Fe_{60}$ (Co–Fe–O)	60° ± 2°	20°	9°	–	84° ± 1°	–
Ceramic	Si_3N_4 (Si_2N_2O/SiO_2)	60° ± 1°	–	4°	–	80° ± 2°	–
	TiO_2	57° ± 1°	3°	6°	–	78° ± 1°	80° ± 2°
	ZnO	74° ± 1°	15°	–	–	82° ± 2°	–
	HfO_2	72° ± 1°	6°	4°	–	80° ± 2°	–
	In–Sn–O	75° ± 1°	3°	4°	3°	79° ± 2°	–
Polymer	Polyimide	71° ± 1°	21°	–	–	79° ± 1°	–

[a] Base pretreatment is the Standard Clean-1 process. [b] Acid pretreatment is treatment with piranha solution.

Figure 3 shows scanning electron microscopy (SEM) images of block copolymer nanotemplates prepared on ruthenium (Ru), Si_3N_4, titania (TiO_2), and cobalt iron alloy ($Co_{40}Fe_{60}$). Figure 3A and B show lamellar nanotemplates assembled upon Ru and Si_3N_4 films. Ru is a highly electric-conductive material frequently applied to the bottom electrode of memory devices. Si_3N_4 is a dielectric material having excellent insulation property and low defect density. The Ru surface was neutrally modified by PETS, and the lamellar period of the block copolymer nanotemplate was 48 nm. The Si_3N_4 substrates were modified by PS-*r*-PMMA, and the lamellar periods of the nanotemplates was 35 nm. The cross-sectional images present surface perpendicular lamellae completely penetrated throughout the film thickness over 60 nm. Note that the lamellar morphology does not appear symmetrical in the SEM images. The imaging contrast for the block copolymer morphology does not originate from chemical distinction between lamellar blocks, but from the topography of block copolymer film induced by beam-damage.[35] Upon SEM observation PMMA component was selectively beam-damaged by electron beam radiation, generating the thin dark part of the SEM images. Figure 3C shows the nanotemplate consisting of surface perpendicular PMMA

© 2008 WILEY-VCH Verlag GmbH & Co. KGaA, Weinheim

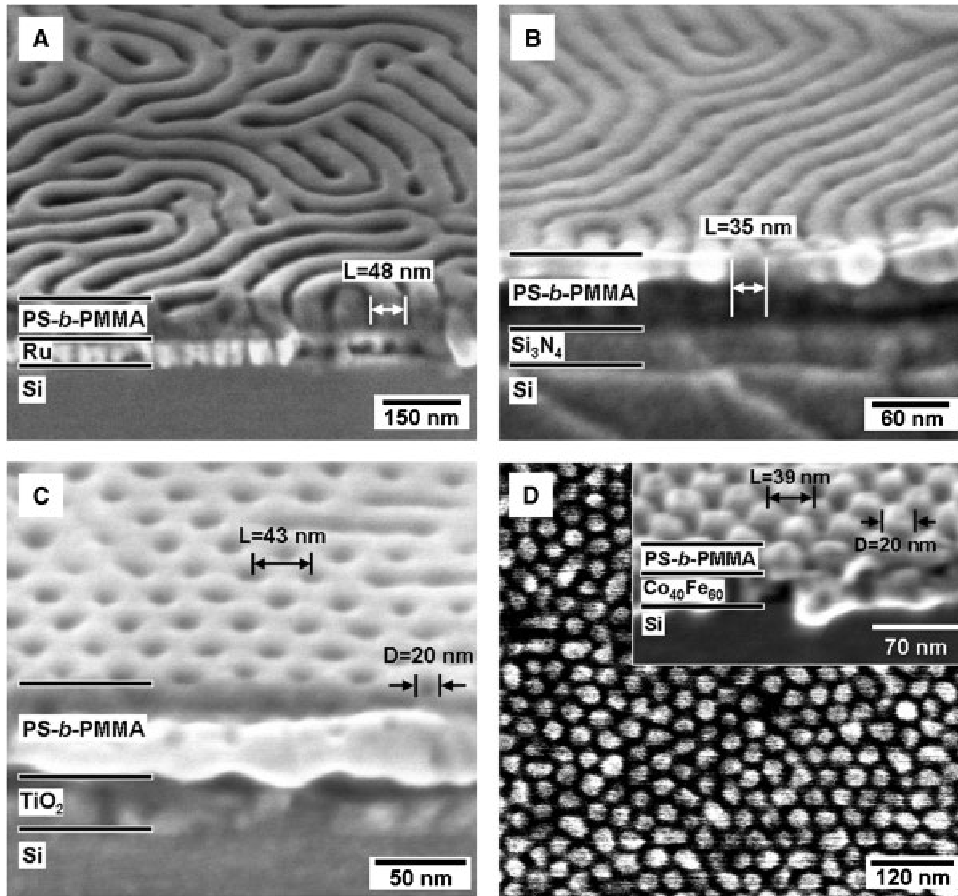

Figure 3. The 45° tilted SEM images of PS-*b*-PMMA lamellar nanotemplates A) on a Ru thin film (lamellar period: 48 nm), and B) on a Si_3N_4 thin film (lamellae period was 35 nm). C) A nanotemplate of surface perpendicular PMMA cylinders in a PS matrix assembled on a TiO_2 film (average diameter of PMMA cylinders: 20 nm, center-to-center distance between neighboring cylinders: 43 nm). D) The plane view and 45° tilted view (inset) of the scanning electron micrographs of a nanotemplate consisting of PS cylinders in a PMMA matrix assembled on a $Co_{40}Fe_{60}$ film (average diameter of the PS cylinders: 20 nm, center-to-center distance between neighboring cylinders: 39 nm).

cylinders in PS matrix assembled upon a TiO_2 substrate. TiO_2 is a semiconductor material with a distinguished photocatalytic property.[6,28] The average diameter of cylinders and the center-to-center distance between neighboring cylinders were 20 nm and 43 nm, respectively. The thickness of the block copolymer thin film was about 65 nm, where the aspect ratio of surface perpendicular cylinders was more than 3. Figure 3D shows the nanotemplates consisting of PS cylinders in PMMA matrix assembled upon a $Co_{40}Fe_{60}$ film. The surface of ferromagnetic alloy[36] was neutrally modified by PS-*r*-PMMA. The average diameter of the PS cylinders was 20 nm, and their center-to-center distance was 39 nm.

The nanoscale morphology of the block copolymer template was transferred into the underlying substrate material by a dry etching process. Metals can be etched by an ion milling process, whereas other materials such as semiconductors, ceramics, and polymers can be etched by RIE. Figure 4 presents the SEM images of the nanostructured films of TiO_2 and Platinum (Pt). In Figure 4A the hexagonal nanoporous TiO_2 film was fabricated by RIE process with CF_4 gas. The average pore diameter and center-to-center distance between them were 20 nm and 43 nm, respectively, which exactly replicated the morphology of a block copolymer nanotemplate with surface perpendicular PMMA cylinders. The large surface area of the nanoporous TiO_2 is anticipated to provide an improved photocatalytic property. Figure 4B and C show nanostructured Pt films prepared by the ion milling

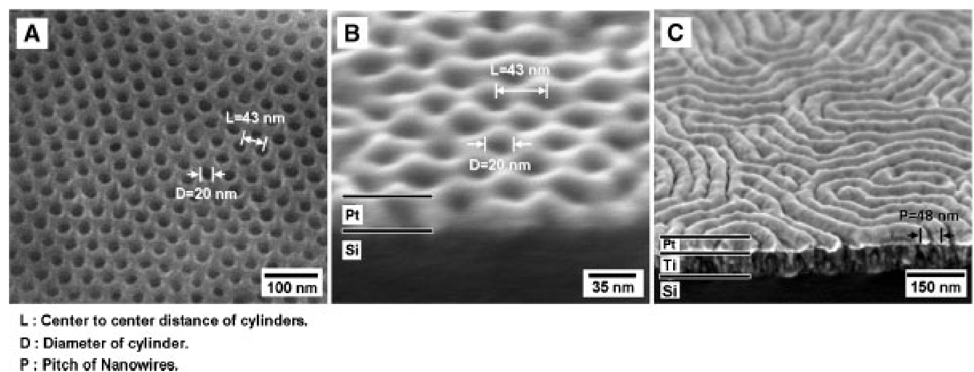

Figure 4. The 45° tilted scanning electron micrographs of A) nanoporous TiO_2 film fabricated by CF_4-RIE process (average pore diameter: 20 nm, center-to-center distance between the pores: 43 nm), and B) nanoporous Pt film, fabricated by Ar^+ ion milling process (average pore diameter: 20 nm, center-to-center distance between the pores: 43 nm). C. The 45° tilted view of scanning electron micrographs of Pt nanowires prepared by Ar^+ ion milling process (stripe pattern pitch: 48 nm, height: 40 nm). Ti film was used as an adhesive layer between the Pt film and Si wafer.

© 2008 WILEY-VCH Verlag GmbH & Co. KGaA, Weinheim

ADVANCED MATERIALS

process. The nanoporous Pt film in Figure 4B is expected to be useful as a high efficiency electrocatalyst for fuel cells due to its large surface area.[37] The Pt nanowires replicating the randomly oriented lamellar morphology of a block copolymer template are potentially applicable to the conductive wires for electronic devices.

In order to achieve the directed assembly into device-oriented well-ordered nanoscale morphology a chemical patterning process has been frequently applied.[18–20] The chemical patterning process is simply applicable to our generalized approach, as shown in Figure 5. Figure 5A schematically depicts the patterning process relying on selective etching or oxidation and the resultant block copolymer morphologies. The cylinders or lamellae align parallel to the selectively etched surface due to a low interfacial tension to the PMMA component. In Figure 5B, the SEM image of a block copolymer film over a broad field shows contrast due to the different orientation of nanoscale morphology. High resolution images of cylindrical (Fig. 5C) and lamellar (Fig. 5D) block copolymers reveal the nanoscale morphology at the boundary between etched and unetched regions, which are consistent to the schematics in Figure 5A. Figure 5E presents ion-milled Pt film, which precisely replicates the nanoscale morphology of a lamellar block copolymer nanotemplate at the boundary between the etched and unetched regions.

In summary, we have demonstrated universal block copolymer lithography for various nanostructured functional materials. As mentioned above, the block copolymer nanotemplates have been mostly applied to silicon substrates and this is largely due to the difficulty in controlling the orientation

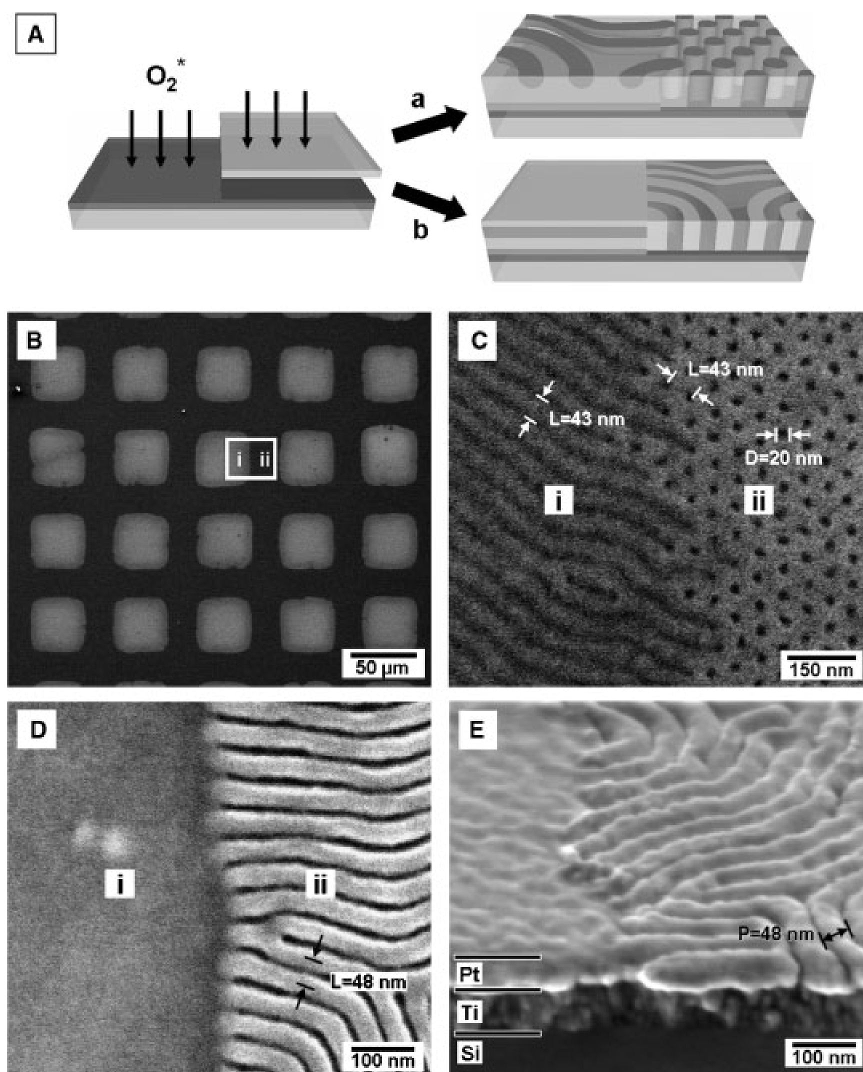

Figure 5. A) Schematic illustration of the chemical patterning process using a TEM grid as an etching mask and the resultant block copolymer morphologies. B) A broad field SEM image of block copolymer thin film upon the edge of the etched region (i: etched region, ii: unetched region). High resolution SEM images of C) cylindrical and D) lamellar block copolymer films at the edge of etched region. E) Nanostructured Pt thin film replicating the morphology of a lamellar block copolymer film at the edge of etched region.

 © 2008 WILEY-VCH Verlag GmbH & Co. KGaA, Weinheim

of those anisotropic nanoscale morphologies on an arbitrary substrate. We have shown that well-ordered block copolymer nanotemplates can be prepared on most of earth's matter, including metals, semiconductors, ceramics, and polymers, provided that the substrate surface has a low surface roughness and sufficient chemical functionality. Owing to the parallel assembly and morphological diversity of block copolymer nanotemplates, our substrate independent nanolithographic process could potentially contribute to the fabrication of numerous nanostructured materials. Further development towards directed assembly upon chemically patterned surfaces[18–22] is anticipated to provide a versatile opportunity to produce well-ordered device-oriented nanostructures of various functional materials.

Experimental

Substrate Preparation: Atomically flat silicon wafers were applied as substrates for film deposition. Pt and $Co_{40}Fe_{60}$ films were deposited by sputtering. Ti (60 nm thickness) was used as an adhesive layer between a metal and Si substrate. The thickness of the deposited films was 40 nm (Pt) and 30 nm ($Co_{40}Fe_{60}$), respectively. Ru, Ir, and HfO_2 films were deposited directly upon Si substrates by PEALD. The film thickness was 60 nm (Ru), 60 nm (Ir), and 35 nm (HfO_2), respectively. TiO_2 film (60 nm thickness) was formed by ALD. Si_3N_4 film (40 nm thickness) was deposited by PECVD. Commercially available In–Sn–O (ITO) glass and polyimide film having a thickness of 200 nm and 25 μm were used as-received. ZnO film was spin-casted using the sol-gel method and had a 60 nm thickness.

Preparation of PS-b-PMMA Nanotemplate: The prepared substrates were pretreated by either ultraviolet oxygen (UVO) radiation or acid or base treatment. The UVO treatment was simply conducted by exposing a substrate to UVO radiation for 20 min. The base treatment was conducted following a standard cleaning procedure in the semiconductor industry as follows. The substrates were cleaned by sequential sonication in CH_2Cl_2, CH_3OH, and H_2O for 10 min each. After washing, they were immersed in a mixture of H_2O_2:NH_4OH:H_2O (vol. ratio: 1:1:5) for 1 h at 100 °C Acid treatment was performed by immersing the substrates in the piranha solution (7:3 mixture of H_2SO_4 and H_2O_2) for 1 h at 110 °C. The pretreated substrates were subsequently washed with deionized water. After the pretreatment process, the substrate surfaces were organically modified by the phenethyltrichlorosilane (PETS) self-assembled monolayer (SAM) or polystyrene-*r*-poly(methyl methacrylate) (PS-*r*-PMMA) random copolymer brush. SAM was deposited by immersing the sample into a 0.1 vol% solution of PETS in toluene for 1 h. The PS-*r*-PMMA brush layer was deposited through spin-casting a thin film of the random copolymer and subsequent thermal annealing at 160 °C for 48 h in a vacuum. After organic treatment, the thin film of the PS-*b*-PMMA diblock copolymer was spin-coated and annealed at a high temperature. A diblock copolymer having the molecular weights of 52000–52000, 25000–26000, 46000–21000, or 20200–50500 for PS and PMMA blocks, respectively, were dissolved in toluene and spin coated over the organically modified substrates. The thermal annealing was conducted at 190 °C for about 40 h to produce a self-assembled nanotemplate. The PMMA component in the nanotemplate was selectively removed by UV exposure and wet-etching in acetic acid. The resultant nanostructured polystyrene template was applied as an etching mask for the further pattern transfer process.

Pattern Transfer: Nanoporous TiO_2 film was prepared by transferring the nanoscale morphology of a block copolymer nanotemplate by CF_4-RIE performed at 50 W RF power and 0.02 Torr. The remaining PS mask was removed by sonicating in toluene. Nanoporous Pt film and Pt nanowires were prepared on ion milling using 400 V Ar^+ at 0.25 mTorr. Residual PS was removed by O_2-RIE at 50 W RF power and 0.07 Torr.

Characterization: Surface roughness (RMS value) was measured by SPA400 Atomic Force Microscopy (Table 1). The water contact angles on the substrate surfaces were measured by Phonenix 150 Contact Angle & Surface Tension Analyzer. The chemical composition of Ir and Si_3N_4 film surfaces was characterized with a VG ESCA2000 X-ray photoelectron spectrometer using an Mg/Al source (Fig. 2). The morphology of the block-copolymer nanotemplates and the fabricated nanostructured films were imaged using a Hitachi S-4800 SEM with a field emission source at 1 kV. The thickness of functional substrates, native oxide layers, and block copolymer nanotemplates was measured using a Woollam M2000D Spectroscopic ellipsometer and K-MAC ST5000_Auto 200 Reflectometer.

Received: November 23, 2007
Revised: December 21, 2007
Published online: April 15, 2008

[1] R. Kelsall, I. Hamley, M. Geoghegan, in *Nanoscale Science and Technology*, Wiley, Chichester, UK **2005**.
[2] G. A. Ozin, A. C. Arsenault, in *Nanochemistry*, Royal Society of Chemistry, Cambridge, UK **2005**.
[3] E. Stern, J. F. Klemic, D. A. Routenberg, P. N. Wyrembak, D. B. Turner-Evans, A. D. Hamilton, D. A. LaVan, T. M. Fahmy, M. A. Reed, *Nature* **2007**, *445*, 519.
[4] Y. Huang, X. Duan, Q. Wei, C. M. Lieber, *Science* **2001**, *291*, 630.
[5] P. P. Pompa, L. Martiradonna, A. D. Torre, F. D. Sala, L. Manna, M. D. Vittorio, F. Calabi, P. Cingolani, R. Rinaldi, *Nat. Nanotechnol.* **2006**, *1*, 126.
[6] R. Sanz, A. Johansson, M. Skupinski, J. Jensen, G. Possnert, M. Boman, M. Vazquez, K. Hjort, *Nano Lett.* **2006**, *6*, 1065.
[7] D. Grosso, C. Boissiere, B. Smarsly, T. Brezesinski, N. Pinna, P. A. Albouy, H. Amenitsch, M. Antonietti, C. Sanchez, *Nat. Mater.* **2004**, *3*, 787.
[8] C. Burda, X. Chen, R. Narayanan, M. A. El-Sayed, *Chem. Rev.* **2005**, *105*, 1025.
[9] B. Lim, A. Rahtu, R. G. Gordon, *Nat. Mater.* **2003**, *2*, 749.
[10] J.-H. Kim, J.-Y. Kim, S.-W. Kang, *J. Appl. Phys.* **2005**, *97*, 093505–2.
[11] Q. Xie, A. Madhukar, P. Chen, N. P. Kobayashi, *Phys. Rev. Lett.* **1995**, *75*, 2542.
[12] S. Donthu, T. Sun, V. Dravid, *Adv. Mater.* **2007**, *19*, 125.
[13] S. Y. Chou, P. R. Krauss, P. J. Renstrom, *Science* **1996**, *272*, 85.
[14] C. R. Martin, *Science* **1994**, *266*, 1961.
[15] T. Shimizu, T. Xie, J. Nishikawa, S. Shingubara, S. Senz, U. Gösele, *Adv. Mater.* **2007**, *19*, 917.
[16] M. Park, C. Harrison, P. M. Chaikin, R. A. Register, D. H. Adamson, *Science* **1997**, *276*, 1401.
[17] T. Thurn-Albrecht, J. Schotter, G. A. Kastle, N. Emley, T. Shibauchi, L. Krusin-Elbaum, K. Guarini, C. T. Black, M. T. Tuominen, T. P. Russell, *Science* **2000**, *290*, 2126.
[18] S. O. Kim, H. H. Solak, M. P. Stoykovich, N. J. Ferrier, J. J. Pablo, P. F. Nealey, *Nature* **2003**, *424*, 411.
[19] M. P. Stoykovich, M. Muller, S. O. Kim, H. H. Solak, E. W. Edwards, J. J. Pablo, P. F. Nealey, *Science* **2005**, *308*, 1442.
[20] S. O. Kim, B. H. Kim, D. Meng, D. O. Shin, C. M. Koo, H. H. Solak, Q. Wang, *Adv. Mater.* **2007**, *19*, 3271.
[21] R. A. Segalman, H. Yokoyama, E. J. Kramer, *Adv. Mater.* **2001**, *13*, 1152.
[22] D. Sundrani, S. B. Darling, S. J. Sibener, *Nano Lett.* **2004**, *4*, 274.
[23] C. T. Black, R. Ruiz, G. Breyta, J. Y. Cheng, M. C. Colburn, K. W. Guarini, H.-C. Kim, Y. Zhang, *IBM J. Res. Dev.* **2007**, *51*, 605.
[24] D. Y. Ryu, K. Shin, E. Drockenmuller, C. J. Hawker, T. P. Russell, *Science* **2005**, *308*, 236.

© 2008 WILEY-VCH Verlag GmbH & Co. KGaA, Weinheim

[25] J. Bang, J. Bae, P. Lowenhielm, C. Spiessberger, S. A. Given-Beck, T. P. Russell, C. J. Hawker, *Adv. Mater.* **2007**, *19*, 4552.
[26] E. Han, I. In, S.-M. Park, Y.-H. La, Y. Wang, P. F. Nealey, P. Gopalan, *Adv. Mater.* **2007**, *19*, 4448.
[27] D. H. Lee, D. O. Shin, W. J. Lee, S. O. Kim, *Adv. Mater.* in press.
[28] R. Wang, K. Hashimoto, A. Fujishima, M. Chikuni, E. Kojima, A. Kitamura, M. Shimohigoshi, T. Watanabe, *Nature* **1997**, *388*, 431.
[29] M. H. Huang, S. Mao, H. Feick, H. Yan, Y. Wu, H. Kind, E. Weber, R. Russo, P. Yang, *Science* **2001**, *292*, 1897.
[30] J. A. Rodriguez, M. Fernandez-Garcia, *Synthesis, Properties, and Applications of Oxide Nanomaterials*, Wiley, Hoboken, NJ **2006**, pp. 1–3.
[31] B. H. Kim, D. O. Shin, S. J. Jeong, C. M. Koo, S. C. Jeon, W. J. Hwang, S. Lee, M. G. Lee, S. O. Kim, *Adv. Mater.*, in press.
[32] P. Mansky, Y. Liu, E. Huang, T. P. Russell, C. Hawker, *Science* **1997**, *275*, 1458.
[33] S. Ardizzone, C. L. Bianchi, G. Cappelletti, M. Ionita, A. Minguzzi, S. Rondinini, A. Vertova, *J. Electroanal. Chem.* **2006**, *589*, 160.
[34] C. Galassi, F. Bertoni, S. Ardizzone, C. L. Bianchi, *J. Mater. Res.* **2000**, *15*, 155.
[35] S. O. Kim, B. H. Kim, K. Kim, C. M. Koo, M. P. Stoykovich, P. F. Nealey, H. H. Solak, *Macromolecules* **2006**, *39*, 5466.
[36] J. S. Mooder, L. R. Kinder, *J. Appl. Phys.* **1996**, *79*, 4724.
[37] X. Peng, K. Koczkur, S. Nigro, A. Chen, *Chem. Commun.* **2004**, *2872.*

© 2008 WILEY-VCH Verlag GmbH & Co. KGaA, Weinheim